The Cryosphere
Discussions

5

Greenland Ice Sheet late-season melt:
Investigating multi-scale drivers of K-transect events

10   Thomas J. Ballinger[1], Thomas L. Mote[2], Kyle Mattingly[2], Angela C. Bliss[3], Edward Hanna[4], Dirk van As[5], Melissa Prieto[1], Saeideh Gharehchahi[1], Xavier Fettweis[6], Brice Noël[7], Paul C.J.P. Smeets[7], Mads H. Ribergaard[8], and John Cappelen[8]

Correspondence to: Thomas J. Ballinger (tballinger@txstate.edu)

15

[1]Department of Geography, Texas State University, San Marcos, TX, USA
[2]Department of Geography, University of Georgia, Athens, GA, USA
[3]College of Earth, Ocean, and Atmospheric Sciences, Oregon State University, Corvallis, OR, USA
[4]School of Geography and Lincoln Centre for Water and Planetary Health, University of Lincoln, Lincoln, UK
20   [5]Geological Survey of Denmark and Greenland, Copenhagen, Denmark
[6]Laboratory of Climatology, Department of Geography, University of Liège, Liège, Belgium
[7]Institute for Marine and Atmospheric Research, Utrecht University, Utrecht, the Netherlands
[8]Danish Meteorological Institute, Copenhagen, Denmark

Abstract. One consequence of recent Arctic warming is an increased occurrence and longer seasonality of above-freezing air temperature episodes. There is significant disagreement in the literature concerning potential physical connectivity between high-latitude open water duration proximate to the Greenland Ice Sheet (GrIS) and unseasonal
30   (i.e. late summer and autumn) GrIS melt events. Here, a new date of sea ice advance (DOA) product is used to determine the occurrence of Baffin Bay sea ice growth along Greenland's west coast for the 2011–2015 period. For the unseasonal melt period preceding the DOA, northwest Atlantic Ocean and atmospheric conditions are analyzed and linked to unseasonal melt events observed at a series of on-ice automatic weather stations (AWS) along the K-transect in southwest Greenland. Mesoscale and synoptic influences on the above and below freezing surface air
35   temperature events are assessed through analyses of AWS wind, pressure, and humidity observations. These surface observations are further compared against Modèle Atmosphérique Régional (MAR), Regional Atmospheric Climate Model (RACMO2), and ERA-Interim reanalysis fields to understand the airmass origins and (thermo)dynamic drivers of the melt events. Results suggest that the K-transect late season, ablation zone melt events are strongly affected by ridging atmospheric circulation patterns that transport warm, moist air from the sub-polar North Atlantic toward west
40   Greenland. While thermal conduction and advection off south Baffin Bay open waters impact coastal air temperatures, consistent with previous studies, marine air incursions from Baffin Bay onto the ice sheet are obstructed by barrier flows and the pressure gradient-driven katabatic regime along the western GrIS margin.

1 Introduction

Significant mass losses in Arctic sea ice and the Greenland Ice Sheet (GrIS) have been observed for the last
four decades (e.g. Serreze and Stroeve, 2015; Bamber et al., 2018). Under sustained climate warming, sea and land
ice have become increasingly sensitive to changes in the frequency and duration of anomalous weather patterns (e.g.
Overland and Wang, 2016; Hanna et al. 2014, 2018b). The Greenland Ice Sheet (GrIS) surface mass balance (SMB)
decrease has contributed roughly 0.5 mm year^{-1} to global mean sea level rise since the early 1990s (van den Broeke et
al., 2016), with about 60% of the mass loss attributed to a decline in SMB and 40% associated with increased ice
discharge (van den Broeke et al., 2017). Observed warming of near-surface west Greenland waters since at least the
early 1990s is linked to accelerated submarine melt and outlet glacier retreat (Holland et al., 2008; Straneo and
Heimbach, 2013) concurrent with a rise in summer warm air temperature extremes along the coast (Hanna et al., 2012,
Mernild et al., 2014). These findings raise the question of whether Baffin local ocean conditions play a key role in
the spatial extent and temporal variations in GrIS melt.

Scholarship published during the past decade has presented conflicting evidence regarding the importance of
the warming of the nearby ocean on GrIS surface melt. Regional modeling experiments have suggested that local sea
surface temperature (SST) impacts on GrIS climate and SMB are negligible due to offshore flow arising from a
prevailing katabatic wind regime (Hanna et al., 2014; Noël et al., 2014). Using a statistical approach, Rennermalm et
al. (2009) found contemporaneous Baffin open water (<15% sea ice concentration (SIC)) and western GrIS melt to be
positively correlated in late summer (1979–2007). The authors noted the strongest, statistically significant correlation
(r=0.71) was observed in August near the K-transect (**Fig. 1**), which was attributed, in part, by wind-driven onshore
transport of warm marine air. Hanna et al. (2009) evaluated lagged correlations between July coastal air temperatures
at Ilulissat and Nuuk (~200 north and south of Kangerlussuaq) from Danish Meteorological Institute (DMI) weather
stations and adjacent, offshore HadISST1 SST values in the preceding and following 2 months. The authors noted a
simultaneous, positive SST relationship with Ilulissat temperatures (r=0.56), while Nuuk temperatures were
significantly coupled with offshore May–July SSTs (r>0.50) over the 1977–2006 record. Ballinger et al. (2018a)
found robust interannual correlations (r>0.40, p≤0.05) during 1979–2014 between Baffin freeze onset dates (from the
Markus et al., 2009 product) and September–December surface air temperatures (SAT) at most DMI stations found
along the west Greenland coastline. The authors found significant, positive Baffin and Labrador SST and coastal SAT
correlations often persist through December after the commencement of freeze onset. Applying a similar correlative
approach and melt/freeze product, Stroeve et al. (2017) showed Baffin and GrIS melt and freeze behaviors to be
synchronous. The authors noted that years with anomalously early sea ice melt tended to have strong, upward
turbulent heat fluxes and westerly winds atop developing open water that transported surplus heat and moisture onto
the ice sheet. Both studies indicate that the synoptic, upper-level circulation pattern is critical for modulating poleward
heat and moisture transport and the surface warming/melt processes at the limits of the melt season. Ballinger et al.
(2018a) proposed a sea ice-heat flux feedback whereby upward turbulent heat fluxes from Baffin Bay help maintain
the high-pressure block aloft, with anticyclonic southerly winds both inhibiting the autumn/winter ice pack formation
and transporting warm marine air onto the western Greenland coast. This potential mechanism may have contributed

to record Greenland Blocking events that occurred in successive years in October during the early-to mid-2000s
80   (Hanna et al., 2018a).

A paucity of research studies focused on the Baffin Bay open water influence on GrIS melt and SMB has
left open the question of potential physical linkages. Our primary goal in this paper is to evaluate and determine
whether the local ocean-atmosphere interactions have played a role in recent, temporally-anomalous GrIS late melt
events spanning the end of summer to freeze-up of adjacent ocean waters. Ice sheet analyses are geographically
85   focused on the western slope of the GrIS with emphasis on the K-transect (**Fig. 1**) as this area – with its two on-ice
automatic weather station (AWS) networks (described in Section 2.1) – is rich with in situ records relative to the
remainder of the ice sheet. We analyze meteorological data from these in situ sources and additionally from regional
climate models and global meteorological re-analyses to address potential links between GrIS late season melt and
the local-scale Baffin marine layer for the period of overlapping data, 2011–2015. For completeness, we subsequently
90   expand the scale of meteorological analyses to consider the influence of greater northwest Atlantic synoptic patterns
on the melt episodes. The paper is organized as follows: Section 2 outlines data sources, Section 3 describes methods
employed, Section 4 covers the local and synoptic scale atmospheric interactions with GrIS melt, Section 5 discusses
key results, and Section 6 offers concluding remarks and makes suggestions for future research.

2 Data

95   **2.1 Passive microwave records**

Sea ice data are from the National Oceanic and Atmospheric Administration/National Snow and Ice Data
Center (NSIDC) Climate Data Record of Passive Microwave SIC v3r1 product distributed by NSIDC (Meier et al.,
2017). We use the "Goddard Merged" SICs that are produced using a combination of the NASA Team and Bootstrap
algorithms applied to satellite passive microwave brightness temperatures (Peng et al., 2013). The data are available
100   daily, 1979–2015, at a 25 km by 25 km nominal grid spacing. The time series of daily SIC at each grid cell were used
to identify the date of sea ice advance (DOA) when SIC increases to 15% for the first time following the sea ice extent
(SIE) minima after Peng et al. (2018). Regional mean DOAs for Baffin Bay were obtained from Bliss et al. (2018, in
review). The local DOA was determined from the time series of SICs between 1 October and 31 March at each grid
cell, then the local mean DOA was computed from 13 grid cells within the domain 66.5 to 67.5°N and 53 to 55°W.
105   SIE was computed by summing the area of grid cells (in km^2) where SIC≥15%. At the same spatial resolution as the
SIC product, the passive microwave daily GrIS melt time series of Mote (2007, 2014) is also used to classify the ice
surface environment in a binary manner (i.e. melt/no melt). Following the Ohmura and Reeh (1991) topographic
regions, we assess GrIS melt conditions on the west-central portion of the ice sheet bounding the K-transect.

2.2 K-transect station data

110   Meteorological conditions from two AWS networks, the Programme for Monitoring of the Greenland Ice
Sheet (PROMICE; stations prefix "KAN") and Utrecht University Institute for Marine and Atmospheric Research
(hereafter IMAU; stations prefix "S"), are used in this study. In order to include the westernmost PROMICE station
KAN_B, analyses begin in 2011 and conclude with the end of the DOA record in 2015. Data are obtained and analyzed
from seven weather stations distributed across the K-transect at ~67°N during this period. The transect spans an area
115   from low-elevation tundra, approximately 1 km inland from the ice sheet glacier terminus (KAN_B), to the lower

accumulation zone (~1800 m) at >140 km from Russell Glacier terminus (KAN_U; see **Fig. 1 & Table 1**). AWS data

used here are recorded at a height of approximately at 2–3 m above the tundra (KAN_B only) or glacial ice surface.

Daily mean air temperature (°C), wind speed (ms^{-1}), and wind direction (0–360°) are obtained from IMAU and

PROMICE station networks. Most data series are complete for the study period, but missing or erroneously low values

120   are filtered out prior to analyses. Additional details on the respective PROMICE and IMAU AWS programs can be

found in van As et al. (2011) and Smeets et al. (2018).

2.3 Atmospheric reanalysis and regional climate model fields

        A number of ERA-Interim reanalysis (Dee et al., 2011) variables are selected for the analysis of atmospheric

conditions across Greenland and the northwestern Atlantic Arctic sector. ERA-Interim surface and upper-air

125   temperatures, wind speeds, and moisture conditions have been shown to exhibit relatively small biases compared to

Arctic observations (Bromwich et al., 2016). MAR and RACMO2, summarized in this section, are also forced with

ERA-Interim fields at their lateral boundaries. Tropospheric winds and specific humidity from 1000-200 hPa are used

to calculate a moisture flux variable known as integrated water vapor transport (IVT); IVT is then classified using a

self-organizing map (SOM) approach (see formal description in the Methods section below). Surface-atmosphere

130   features and regional circulation are further evaluated using latent and sensible heat flux data, 500 hPa geopotential

heights (GPH), and 1000-700 hPa mean winds at the native 80 km resolution.

        Model output u,v wind speed and direction at 10-m and 850 hPa from MAR and RACMO2 are evaluated to

understand low-level flow over ocean-land-ice sheet areas surrounding the K-transect. Secondarily, we briefly discuss

inter-model differences within the planetary boundary layer and biases against AWS observations. Both regional

135   climate models are specifically developed for simulating polar weather and climate, in particular over the Greenland

ice sheet (e.g., Fettweis et al., 2011; Noël et al., 2018). MAR v3.9 fields at 15 km are used here (see Fettweis et al.

2017 for a detailed model description). Relative to MAR v3.8 used in Delhasse et al. (2018), the main changes to

MAR v3.9 consist of enhanced computational efficiency, adjustments to some of the snow model parameters to better

compare with in situ observations, and improved MAR dynamical stability by increasing the atmospheric filtering.

140   RACMO2.3p2 fields at a horizontal resolution of 5.5 km are also used (Noël et al., 2018). Model physics have not

changed relative to the previous 11 km version described in Noël et al. (2018). The refined spatial resolution of the

host model improves the depiction of topographically complex terrain at the GrIS margins such as small peripheral

glaciers and ice caps, improving the representation of near-surface, local winds.

2.4 North Atlantic atmospheric indices

145   Daily atmospheric indices are examined to characterize surface and upper-level conditions within a historical

context. The Greenland Blocking Index (GBI) (Hanna et al., 2018) describes daily mean 500 hPa geopotential height

values from 60-80°N and 20-80°W. The North Atlantic Oscillation (NAO) index used here is adapted from Cropper

et al. (2015) and represents station-based daily mean sea-level pressure differences between Iceland and the Azores.

Both versions of the respective indices are normalized by their day of year means and standard deviations for the

150   common 1951–2000 base period.

3 Methods

A composite approach is applied to characterize atmospheric conditions underlying unseasonal GrIS melt events, defined here as occurring at the conclusion of boreal summer (i.e. late August) and during autumn preceding sea ice advance on Baffin Bay (**Table S1**). Two constraints are placed on the composite analyses. First, the technique

155　is intended to isolate regional meteorological processes during KAN_B air temperature events of ≥0°C (T+) versus <0°C (T-). KAN_B is selected to build composite sizes as this location experiences more T+ events annually than any other PROMICE or IMAU AWS on the K-transect, and due to station's location near the ice margin along the transect (**Table 1**). T+ comparisons between the KAN_B and other K-transect stations are provided in **Table 2**. The second limit involves the length of the analysis period prior to DOA. Through lead/lag correlations of recent data

160　series of ≥30 years, Hanna et al. (2009) and Ballinger et al. (2018a) noted Baffin ice coverage and sea surface temperatures in the preceding two months to be positively and significantly correlated with west Greenland coastal air temperature variations. Composites here are constructed over a similar two-month (60-day) period with data additionally sub-divided into 60-31 day (i.e. D_{60}) and 30-1 day (i.e. D_{30}) bins preceding each Baffin DOA from 2011 to 2015. A paucity of T+ events over the 30 days post-Baffin DOA limits analyses to the aforementioned periods

165　before the development of extensive, seasonal sea ice coverage.

In a similar fashion to Carr et al. (2017), a Wilcoxon test is utilized to evaluate differences in atmospheric variables and indices between T+ versus T- events. This nonparametric test is intended for continuous data series that do not follow underlying assumptions of the normal distribution making it appropriate for comparative analyses between extreme and non-extreme conditions. The null hypothesis of no difference in atmospheric conditions between

170　cases is rejected at the 95% confidence level when p≤0.05.

Following Mattingly et al. (2016, 2018), daily atmospheric moisture transport about Greenland is resolved by calculating integrated water vapor transport (IVT) as in Eq. (1):

$$IVT = \frac{1}{g} \int_{1000 \text{ hPa}}^{200 \text{ hPa}} qV \, dp \qquad \qquad (1)$$

where g is gravitational acceleration, q is specific humidity, V is the vector wind (ms⁻¹), and dp represents the

175　difference between atmospheric pressure levels. The percentile rank of IVT (IVT PR) within a 30-day moving window is calculated to account for the seasonal cycle of IVT, and IVT PR is then classified using the SOM technique to produce a matrix of moisture transport patterns, or nodes, that typically occur over the Greenland region. As in Mattingly et al. (2016), similar wet (anomalously high), neutral (near climatological median values), and dry (anomalously low) IVT patterns are aggregated, then their frequencies are composited and tested following methods

180　previously summarized.

4 Results

4.1 Characteristics of Baffin and west Greenland late season melt

Perspectives on the end of the Northwest Atlantic melt season area are shown in **Fig. S1**. Slow, upward change signifying later sea ice formation is shown in the DOA series, particularly from around 2000. Meanwhile, the

185　start of the last ≥3-day sequence of Region 3 (west-central Greenland; see inset in **Fig. 1**) 2% or 4% melt area also suggest progressively later melt (and a later onset of the freeze season). A significant break in the 2% series is highlighted by a drastic increase in variability from 1979–1999 (σ=21.17) to 2000–2015 (σ=44.25) that also presents in the annual discharge records from the nearby Watson River and Tasersiaq ice sheet catchments (Ahlstrøm et al.,

2017; van As et al., 2018). Differences between the beginning of Baffin Bay sea ice advance and the end of the ice

190   sheet melt season has clearly narrowed, and some GrIS melt events since 2000 have occurred after seasonal sea ice formation (i.e. 2002, 2004–2005, 2010).

Relative to the climatology defined as 1981–2010, sea ice advanced ~11d earlier in 2011 and ~6d later than the mean date in 2012–2015 (**Table S1**). Inspection of DOA for individual grid cells adjacent to the Sisimiut AWS (WMO code 4234 in **Fig. 1**), located ~150 km west of the K-transect ice sheet margin, reveals a northward-extending

195   notch where ice forms ~30–60d later than the Baffin-wide DOA (**Fig S2a-e**; **Fig S3**). Interannual differences in ice cover advance often depend on factors including regional winds, ocean heat transport, and water-mass changes (Myers et al., 2009; Ribergaard, 2014). For instance, strong offshore winds and poleward circulation of warm water from the West Greenland Slope Current (WGSC) often contribute to the local open water persistence, while southward Arctic Water transports support earlier ice formation patterns found in the east and north (Curry et al., 2014).

200   **4.2 Local meteorology of melt versus non-melt cases**

The spatial coherence of observations across the K-transect along with inhomogenous GrIS Region 3 spatial melt patterns and satellite pixel contamination issues at the tundra-ice interface, lead us to assess the melt events at the station level. Composites of air temperature, wind speed and direction by KAN_B T+ and T- events are shown in **Fig. 2**. Across the transect, composite air temperature differences (T+ versus T- events) are warmer by roughly 7 to

205   8°C in the D_{60} window and 12 to 13°C in the D_{30} period (**Fig. 2a**). These differences tend to be least near the coast and increase to S6 in the mid-ablation area (~1000 m asl) where contemporaneous melt occurs ~14–16% of the time (**Table 2**).

Wind direction for T+ events is consistently SSE (<150°) in D_{60} and comparatively becomes slightly more southerly in the D_{30} period (**Fig. 2c**) regardless of the wind speed (**Fig. 2b,d**). Differences in wind direction do not

210   strongly change by temperature regime, but there is evidence of slight wind speed intensification during D_{60} T+ events (~1–2 ms^{-1}) and to a lesser magnitude similar relationships hold during the D_{30} period (**Fig. 2b**). Increased winds reflect strengthened ESE katabatic flows as the result of seaward enhancement of the pressure gradient (not shown) from nearshore open water persistence, increased synoptic cyclone activity, and lower MSLP over Baffin Bay during the summer-autumn season transition (McLeod and Mote, 2015). Wind speed increases also initiate positive (upward)

215   sensible heat fluxes and convective boundary layer intensification associated with low elevation ice melt (**Fig. S4**). Just offshore, sensible and latent fluxes are generally negative in T- events and near zero to slightly positive in melt occurrences with large, positive differences in T+ vs T- events apparent in oceanic areas from the Labrador Sea extending up to the WGSC (**Figs. S4** and **S5**).

Offshore flows appear to represent a dynamic barrier to Baffin marine layer intrusions. To further examine

220   lower tropospheric flow across the ocean-land-ice interface, we similarly composite MAR and RACMO2 winds at 10-m and 850 hPa (**Figs. 3** and **4**). In general, the MAR and RACMO2 winds show directional consistency with overlaid PROMICE and IMAU winds with a slight southerly bias in both products for D_{30} at KAN_M and S9. Modeled wind speeds are more intense during T+ versus T- events as corroborated in observations with pressure gradient enhancement, positive surface radiative balance, and katabatic (or glacier) wind presence near the ice margin

225   in summer and early autumn (van den Broeke et al., 2009). T+ events in RACMO2 and MAR generally capture AWS

observed wind speeds in the upper ablation zone at KAN_M ($r^2 \geq 0.77$) and lower accumulation zone at KAN_U ($r^2 \geq 0.77$) with low root mean squared errors (not shown). A slight, positive bias in both models is evident at the ice sheet edge near KAN_B (MAR $r^2 = 0.33$, RACMO2 $r^2 = 0.58$). Height differences between the AWS measurements (2–3 m) and model outputs (10-m) may explain a portion of the bias at KAN_B. Except during D_{30} T+ events, the 10-

230   m winds extending about the transect from the west coast tundra just offshore and into eastern Baffin Bay are notably calm and alongshore (i.e. northerly in T- and southerly in T+; **Figs. 3** and **4**).

4.3 The role of North Atlantic atmospheric patterns

Composites of the AWS K-transect observations and complementary regional model output suggest that late season melt inferred from T+ events may be driven by synoptic patterns as opposed to local marine forcing. Overplots

235   of 500 hPa GPH, 1000-700 hPa mean wind, and IVT for the North Atlantic region are shown in **Fig. 5**. Whereas T-events (left panels) tend to be characterized by northerly winds over the 1000-700 hPa layer, the T+ events (right panels) indicate southerly, on-ice transfer of subpolar air aided by the presence of an upper-level trough over Baffin Island and downwind ridging over Greenland. Comparatively higher GPH values are found over ice sheet with the 540 dam (i.e. 5400 m) contour extending across central Greenland in T+ events, but located south of the island in T-

240   events. In both T+ cases, low-level winds circulate poleward over north Labrador Sea areas of upward, turbulent heat flux (**Figs. S4** and **S5**), aiding the heat and moisture transfer (as shown by heightened IVT values in T+ relative to T-) over western Greenland during D_{60} and D_{30} (**Fig. 5**). Local IVT maxima in both events are concentrated over the southwest tip of the island, but remain ~100 kg m^{-1} s^{-1} or higher near the K-transect. Comparatively, depth integrated moisture flux over much of the west coast increases by a factor of 2–3 (4–5) during D_{60} (D_{30}) T+ versus T- events

245   signaling a concentration of moist, onshore flow that drives the above-freezing air temperatures.

To further characterize and differentiate weather conditions by T± event, we composite SOM-classified daily IVT wet, dry, and neutral patterns identified by Mattingly et al. (2016). Analyses of the aggregated frequencies suggest that the wet patterns (with anomalously high IVT versus climatology) occur significantly more often in T+ versus T- events, and such nodes are more common by a factor of >4.5 in the D_{30} period. (**Fig. 6a**). While some

250   caution should be exercised as the absolute frequency of these patterns decreases from roughly early (D_{60}) to late (D_{30}) autumn, humid atmospheric conditions appear to enhance unseasonal melt. Increased incidence of wet patterns coincides with negative (positive) NAO (GBI) (both >|0.50| in T+ events; **Fig. 6b**), and a synoptic environment characterized by high surface (upper-level) pressure anomalies. This is confirmed by **Fig. 5** whereby the higher 500 GPH values and on-ice lower tropospheric mean winds in T+ events transport moist air masses from Labrador Sea

255   and southerly maritime latitudes to much of the western slope of the ice sheet to facilitate ablation-area melt.

5 Discussion

West Greenland summer and autumn air temperature variability and trends during the last 3–4 decades have shown strong response to increased Greenland high-pressure blocking intensity and North Atlantic SSTs aided by background anthropogenic forcing (Hanna et al., 2016; McLeod and Mote, 2016; Ballinger et al., 2018a; Graeter et

260   al., 2018). The current North Atlantic "warm period" since the mid-1990s is characterized by a positive Atlantic Multidecadal Oscillation phase and rising SSTs around southwestern Greenland (Myers et al., 2009; Ribergaard, 2014), including just offshore of Sisimiut (WMO code 4234 in **Fig. 1**) (orthogonal trend = +0.03°C year^{-1}, p<0.05, for

1995-2015 period using SST product described in Ballinger et al., 2018b). Warming waters around the island are influencing Baffin sea ice and west GrIS melt processes (Hanna et al., 2013; McLeod and Mote, 2015; Ballinger et al., 2018a) and seasonality toward earlier (later) melt (freeze) (Stroeve et al., 2017). This hotspot of melt about K-transect suggests local low SIC and/or open water and inferred upward turbulent heating atmospheric could influence nearby terrestrial melt events. As shown in **Fig. S6**, Sisimiut SSTs fluctuate with air temperatures (over the 60 days preceding DOA) in a statistically significant fashion for 2013-2015 at most K-transect stations with some distance decay noted toward the edge of the ablation zone at S9. Summer and autumn west Greenland near-coastal air temperatures have been shown to be modulated by the thermal properties of bordering SSTs (Hanna et al., 2009; Ballinger et al., 2018a). Interannual differences in the strength of SST-air temperature relationships (i.e. 2013–2015 versus 2011–2012) suggest: 1) processes driving warming ocean waters and air temperatures over the GrIS are independent when disparate wind directions occur at or near the ocean-tundra-ice sheet boundaries in years of weak-to-zero correlation (e.g. katabatic flows contrasting near-coastal barrier flows (van den Broeke and Gallée, 1996)), or alternatively 2) strong large-scale atmospheric circulation forcing in years of positive, often statistically robust co-variability (i.e. near-surface and upper-level meridional winds) modulates the near-shore surface open water and ice sheet air temperatures (Stroeve et al., 2017). We recognize that synoptic patterns may not necessarily be mutually exclusive in these examples, but the manuscript objectives do not include comparison of high and low pressure features around Greenland for specific melt and non-melt events.

A number of studies have suggested that Baffin marine layer interaction with the ice sheet boundary layer is obstructed by zonal and meridional flows such as the west coast plateau jet feature and katabatic winds (Hanna et al., 2009; Moore et al., 2013; Noël et al., 2014). Moore et al. (2013) noted a directionally consistent southerly 10-m wind field extending over the western half of Greenland in summer and winter, while observational studies similarly indicate a high frequency of southerly-to-southeasterly winds over the K-transect (van den Broeke et al., 2009). Southerly (easterly) 10-m winds are strongly linked to melt across two thirds (the southern third) of the ice sheet (Cullather and Nowicki, 2018). For an expanded spatial perspective, we briefly examine air temperatures at the next PROMICE station installment north at Upernavik (UPE; 72.89°N). We find UPE_L (220 m asl on the ice sheet) melt occurs the day of KAN_B T+ events on >50% of occasions in both D_{60} and D_{30} windows (not shown). This suggests that above-freezing near-surface air penetrates at least to PROMICE station UPE_L with a relatively warm air mass engulfing much of the west coast. Our observational and regional model analyses further show that homogenous low-level winds extend coastward at least to the tundra-ice sheet interface near KAN_B (see **Figs. 2c**, **3**, and **4**) and produce a "blocking effect" that inhibits the inland penetration of near-surface Baffin air (Noël et al., 2014). Of note, the katabatic wind mechanism becomes stronger and therefore more preventative of local marine influence with increased radiative cooling toward the Baffin DOA and continuous freeze period in climatological winter (van As et al., 2014).

If late season K-transect melt does not appear to be driven by a local Baffin influence, then what physical mechanisms drive the melt events? We show that T+ events by D_{60} and D_{30} partitions are characterized by southerly flows of more warm, moist maritime air of lower latitude origins relative to T- cases. As shown in **Fig. 5**, during the former event period, air is transferred off northern Labrador Sea to the west coast, while a path of more southerly flow directs moist North Atlantic air masses onto Baffin Bay and southwestern Greenland in the period immediately

300   preceding DOA. These "wet" synoptic patterns occur frequently under anomalous ($>|1\sigma|$) positive (negative) GBI
        (NAO) values (**Fig. 6a**, **b**). We surmise from Mattingly et al. (2018) that such patterns are particularly moisture-rich
        ($\geq85^{th}$ percentile IVT climatological values) and often accompanied by atmospheric rivers impacting Greenland, and
        their occurrence causes ablation zone melt in non-summer months through cloud radiative effects, condensational
        latent heat release, and liquid precipitation (Doyle et al., 2015; Binder et al., 2017; Oltmanns et al., 2018). The
305   southerly winds that propagate moisture northward are a product of amplified upper-level heights in T+ versus T-
        events extending from Denmark Strait and Irminger Sea onto the ice sheet (**Fig. 5**). Mid-tropospheric ridging, which
        is more pronounced in D_{30} events, supports southerly winds that funnel heat and moisture across Baffin Bay and
        southwest Greenland to stimulate sea ice and GrIS ablation area melt conditions (Ahlstrøm et al., 2017; Ballinger et
        al., 2018a,b; Hanna et al., 2018). Cullather and Nowicki (2018) similarly find collocated, positive surface and 500
310   hPa GPH anomalies over Denmark Strait and Irminger Sea tend to be associated with melt events in the basin
        encompassing the K-transect. Our analyses support North Atlantic-air-ice sheet coupling, rather than localized Baffin
        ocean-atmosphere processes, as a strong driver of transition season melt before sea ice advances south of the K-
        transect. Synoptic patterns associated with negative summer NAO and positive GBI incidence strongly influence
        these melt events (**Fig. 6**), prompting decreases in SMB, and increase in the K-transect equilibrium line altitude over
315   the last 10-15 years (Hanna et al., 2013; Smeets et al., 2018).

6 Conclusions

        Temporal co-variability between GrIS and Arctic sea ice mass loss suggests a possible feedback whereby
        adjacent open water conditions, ocean-to-atmosphere heat flux, and on-ice winds affect inland melt during summer
        (Rennermalm et al., 2009; Liu et al., 2016) and around the limits of the melt season (Stroeve et al., 2017). In our
320   2011–2015 analyses bridging the end-of-summer/early autumn melt to the date of first-year Baffin sea ice advance,
        we find no evidence to support the hypothesis that local open water and resultant turbulent heating has a demonstrable
        impact on inland ice melt events. These thermodynamic processes directly influence coastal air temperatures and have
        a fingerprint on marine outlet glacier behaviors (Carr et al., 2017), but are shown here to be inhibited by
        topographically-influenced flows and synoptic patterns whose interactions are not mutually exclusive. Furthermore,
325   Baffin Bay warming coupled with a longer autumn open water period has been hypothesized to stimulate and
        invigorate upper-level, high-pressure blocking that promotes southerly air advection over the west Greenland coast
        (Ballinger et al., 2018a). This is consistent with the main conclusions of Noël et al. (2014), which suggest that while
        warming waters around Greenland minimally effect SMB beyond enhancing tidewater glacier retreat rates SST forcing
        may indirectly effect GrIS SMB changes through impacts on atmospheric circulation. Thus in terms of direct forcing,
330   beyond a near-coastal influence, we find that Baffin Bay does not represent an advective heat and moisture source to
        the ice sheet during our 5-year analyses.

        Future late season analyses, perhaps reconstructing K-transect meteorological conditions back to the origins
        of the modern sea ice record, might be insightful in comparing local ocean-ice sheet interactions spanning the 1990s
        shift from colder to warmer Baffin summer SSTs (Ballinger et al., 2018a). Temperature and pressure gradients derived
335   from retrospective analyses would also be useful to categorize the magnitude and direction of regional winds,
        including the katabatic regime, in attempting to provide a longer-term perspective of analyses presented in this paper.

Noël et al. (2014) hypothesized that future sea-surface warming may exacerbate the division between local ocean and ice sheet by intensifying the temperature and pressure gradient and hence resulting katabatic winds. Baffin Bay climate and cryospheric changes in the last two decades suggest such an increased "blocking" mechanism may already

340   be underway. Moreover, stronger katabatic winds might be enhanced further by an increasing intensity of autumn mid-troposphere high-pressure over Greenland (Hanna et al., 2018a, see their Fig. 1e). Synergistic future research should continue to monitor the spatial extent, drivers, and physical effects of unseasonal melt through observational products and regional modeling tools, including quantification of late season K-transect mass loss and runoff through the Watson River, contributions to subsurface/firn processes, and preconditioning effects on the following year's melt

345   season.

References

Ahlstrøm, A.P., Petersen, D., Langen P.L., Citterio, M., and Box, J.E.: Abrupt shift in the observed runoff from the southwestern Greenland ice sheet. Sci. Advan., 3, 1-7, doi:10.1126/sciadv.1701169, 2017.

365 Ballinger, T.J., Hanna, E., Hall, R.J. Miller, J., Ribergaard, M.H., and Høyer, J.L.: Greenland coastal air temperatures linked to Baffin Bay and Greenland Sea ice conditions during autumn through regional blocking patterns. Clim. Dyn., 50, 83-100, doi:10.1007/s00382-017-3583-3, 2018a.

Ballinger, T.J., Hanna, E., Hall, R.J., Miller, J., Ribergaard, M.H., Overland, J.E., and Høyer, J.L.: Anomalous blocking over Greenland preceded the 2013 extreme early melt of local sea ice. Ann. Glaciol., 59, 181-190,
370 doi:10.1017/aog.2017.30, 2018b.

Bamber, J.L., Westaway, R.M., Marzeion, B. and Wouters, B.: The land ice contribution to sea level during the satellite era. Environ. Res. Lett. 13, 063008, doi:10.1088/1748-9326/aac2f0, 2018.

Binder, H., Boettcher, M., Grams, C.M., Joos, H., and Wernli, H.: Exceptional air mass transport and dynamical drivers of an extreme wintertime Arctic warm event. Geophys. Res. Lett., 44, 12028-12036,
375 doi:10.1002/2017GL075841, 2017.

Bliss, A. C., Steele, M., Peng, G., Meier, W.N., and Dickinson, S.: Regional Variability of Arctic Sea Ice Seasonal Change Climate Indicators from a Passive Microwave Climate Data Record, Environ. Res. Lett., 2018, in review.

Bromwich, D.H., Wilson, A.B., Bai, L.-S., Moore, G.W.K., and Bauer, P.: A comparison of the regional Arctic System Reanalysis and the global ERA-Interim Reanalysis for the Arctic. Q.J.R. Meteorol. Soc., 142, 644-658,
380 doi:10.1002/qj.2527, 2016.

Cappelen, J.: Weather observations from Greenland 1958-2017. Observation data with description. DMI Report 18-08. Copenhagen, Denmark, 2018.

Cappelen, J.: Weather observations from Greenland 1958-2018. Observation data with description. DMI Report 19-08. Copenhagen, Denmark, 2019, in preparation.

385 Carr, J.R., Stokes, C.R., and Vieli, A.S.: Threefold increase in marine-terminating outlet glacier retreat rates across the Atlantic Arctic: 1992-2010. Ann. Glaciol., 58, 72-91, doi:10.1017/aog.2017.3, 2017.

Cropper, T., Hanna, E. Valente, M.A., and Jónsson, T.: A daily Azores-Iceland North Atlantic Oscillation index back to 1850. Geosci. Data J., 2, 12-24, doi:10.1002/gdj3.23, 2015.

Cullather, R.I., and Nowicki, S.M.J.: Greenland ice sheet surface melt and its relation to daily atmospheric conditions.
390 J. Clim., 31, 1897-1919, doi:10.1175/JCLI-D-17-0447.1, 2018.

Curry, B. Lee, C.M., Petrie, B., Moritz, R.E., and Kwok, R.: Multiyear volume, liquid freshwater, and sea ice transports through Davis Strait, 2004-2010. J. Phys. Oceanog., 44, 1244-1266, doi:10.1175/JPO-D-13-0177.1, 2014.

Dee, D.P., Uppala, S.M., Simmons, A.J., Berrisford, P., Poli, P., Kobayashi, S., Andrae, U., Balmaseda, M.A.,
395 Balsamo, G., Bauer, P., Bechtold, P., Beljaars, A.C.M., van de Berg, L., Bidlot, J., Bormann, N., Delsol, C., Dragani, R., Fuentes, M., Geer, A.J., Haimberger, L., Healy, S.B., Hersbach, H., Hólm, E.V., Isaksen, L., Kållberg, P., Köhler, M., Matricardi, M., McNally, A.P., Monge-Sanz, B.M., Morcrette, J.-J., Park, B.K., Peubey, C., de Rosnay, P., Tavolato, C., Thépaut, J.-N., Vitart, F.: The ERA-Interim reanalysis: configuration

and performance of the data assimilation system. Q. J. R. Meteorol. Soc., 137, 553–597, doi:10.1002/qj.828,
400   2011.

Delhasse, A., Fettweis, X., Kittel, C., Amory, C., and Agosta, C.: Brief communication: Impact of the recent
atmospheric circulation change in summer on the future surface mass balance of the Greenland Ice Sheet,
Cryosphere, 12, 3409-3418, doi:10.5194/tc-2018-65, 2018.

Doyle, S., Hubbard, A., van de Wal, R.S., Box, J., van As, D., Scharrer, K., Meierbachtol, T.W., Smeets, P.C.J.P.,
405   Harper, J.T., Johansson, E., Mottram, R.H., Mikkelsen, A.B., Wilhelms, F., Patton, H., Christoffersen, P.,
Hubbard, B.: Amplified melt and flow of the Greenland ice sheet driven by late-summer cyclonic rainfall. Nat.
Geosci. 8, 647-653, doi:10.1038/ngeo2482, 2015.

Fettweis, X., Tedesco, M., van den Broeke, M., and Ettema, J.: Melting trends over the Greenland ice sheet (1958–
2009) from spaceborne microwave data and regional climate models, Cryosphere, 5, 359-375, doi:10.5194/tc-5-
410   359, 2011.

Fettweis, X., Box, J. E., Agosta, C., Amory, C., Kittel, C., Lang, C., van As, D., Machguth, H., and Gallée, H.:
Reconstructions of the 1900–2015 Greenland ice sheet surface mass balance using the regional climate MAR
model, Cryosphere, 11, 1015-1033, doi:10.5194/tc-11-1015, 2017.

Graeter, K.A., Osterberg, E.C., Ferris, D.G., Hawley, R.L., Marshall, H.P., Lewis, G., Meehan, T., McCarthy, F.,
415   Overly, T., and Birkel, S.D.: Ice core records of west Greenland melt and climate forcing. Geophys. Res. Lett.,
45, 3164-3172, doi:10.1002/2017GL076641, 2018.

Graham, R.M., Cohen, L., Petty, A.A., Boisvert, L.N., Rinke, A., Hudson, S.R., Nicolaus, M., and Granskog, M.A.:
Increasing frequency and duration of Arctic winter warming events. Geophys. Res. Lett., 44, 6974-6983,
doi:10.1002/2017GL073395, 2017.

420   Hanna, E. Cappelen, J., Fettweis, X., Huybrechts, P., Luckman, A., and Ribergaard, M.H.: Hydrologic response of the
Greenland ice sheet: the role of oceanographic warming. Hydrol. Proc., 23, 7-30, doi:10.1002/hyp.7090, 2009.

Hanna, E., Mernild, S.H., Cappelen, J., and Steffen, K.: Recent warming in Greenland in a long-term instrumental
(1881-2012) climatic context: I. Evaluation of surface air temperature records. Environ. Res. Lett., 7, 1-15,
doi:10.1088/1748-9326/7/4/045404, 2012.

425   Hanna, E., Jones, J.M., Cappelen, J., Mernild, S.H., Wood, L., Steffen, K., and Huybrechts, P.: The influence of North
Atlantic atmospheric and oceanic forcing effects on 1900-2010 Greenland summer climate and ice melt/runoff.
Int. J. Climatol., 33, 862-880, doi:10.1002/joc.3475, 2013.

Hanna, E., Fettweis, X., Mernild, S.H., Cappelen, J., Ribergaard, M.H., Shuman, C.A., Steffen, K., Wood, L., and
Mote, T.L.: Atmospheric and oceanic climate forcing of the exception Greenland ice sheet surface melt in
430   summer 2012. Int. J. Climatol., 34, 1022-1037, 2014.

Hanna, E., Cropper, T.E., Hall, R.J., and Cappelen, J.: Greenland Blocking Index 1851–2015: a regional climate
change signal. Int. J. Climatol., 36, 4847-4861, doi:10.1002/joc.4673, 2016.

Hanna E., Hall, R.J., Cropper, T.E., Ballinger, T.J., Wake, L., Mote, T., and Cappelen, J.: Greenland Blocking Index
daily series 1851-2015: analysis of changes in extremes and links with North Atlantic and UK climate variability
435   and change. Int. J. Climatol., 38, 3546-3564, doi:10.1002/joc.5516, 2018a.

Hanna, E., Fettweis, X., and Hall, R.J.: Brief communication: Recent changes in summer Greenland blocking captured by none of the CMIP5 models. Cryosphere, 12, 3287-3292, doi:10.5194/tc-12-3287, 2018b.

Holland, D.M., Thomas, R.H., de Young, B., Ribergaard, M.H., and Lybert, B.: Acceleration of Jakobshavn Isbrae triggered by warm subsurface ocean waters. Nat. Geoscience, 1, 659-664, doi:10.1038/ngeo316, 2008.

440   Liu, J., Chen, Z., Francis, J., Song, M., Mote, T., and Hu, Y: Has Arctic sea ice loss contributed to increased surface melting of the Greenland ice sheet? J. Clim., 29, 3373-3386, doi:10.1175/JCLI-D-15-0391.1, 2016.

Markus, T., Stroeve, J. C., and Miller, J.: Recent changes in Arctic sea ice melt onset, freeze-up, and melt season length. J. Geophys. Res., 114, C12024, doi:10.1029/2009JC005436, 2009.

Mattingly, K.S., Ramseyer, C.A., Rosen, J.J., Mote, T.L., and Muthyala, R.: Increasing water vapor transport to
445   Greenland Ice Sheet revealed using self-organizing maps. Geophys. Res. Lett., 43, 9250-9258, doi:10.1002/2016GL070424, 2016.

Mattingly, K.S., Mote, T.L., and Fettweis, X.L.: Atmospheric river impacts on Greenland ice sheet surface mass balance. J. Geophys. Res. Atmos., 123, 8538-8560, doi:10.1029/2018JD028714, 2018.

McLeod, J.T., and Mote, T.L.: Assessing the role of precursor cyclones on the formation of extreme Greenland
450   blocking episodes and their impact on summer melting across the Greenland ice sheet. J. Geophys. Res., 120, 12357-12377, doi:10.1002/2015JD023945, 2015.

McLeod, J.T., and Mote, T.L.: Linking interannual variability in extreme Greenland blocking episodes to the recent increase in summer melting across the Greenland ice sheet. Int. J. Climatol., 36, 1484-1499, doi:10.1002/joc.4440, 2016.

455   Meier, W., Fetterer, F., Savoie, M., Mallory, S., Duerr, R., and Stroeve, J.: NOAA/NSIDC Climate Data Record of Passive Microwave Sea Ice Concentration, Version 3, Revision 1, National Snow & Ice Data Center, Boulder, Colorado (Accessed 18 December 2017), doi:http://dx.doi.org/10.7265/N59P2ZTG, 2017.

Mernild, S.H., Hanna, E., Yde, J.C., Cappelen, J., and Malmros, J.K.: Coastal Greenland air temperature extremes and trends 1890-2010: annual and monthly analysis. Int. J. Climatol., 34, 1472-1487, doi:10.1002/joc.3777, 2014.

460   Moore, G.W.K., Renfrew, I.A., and Cassano, J.J.: Greenland plateau jets. Tellus A, 65, 1748, 1-16, doi:10.3402/tellusa.v65i0.17468, 2013.

Moore, G.W.K.: The December 2015 North Pole Warming Event and increasing occurrence of such events. Sci. Rep., 6, 39084, doi:10.1038/srep39084, 2016.

Mote, T.L.: Greenland surface melt trends 1979-2007: Evidence of a large increase in 2007. Geophys. Res. Lett., 34,
465   L22507, doi:10.1029/2007GL0311976, 2007.

Mote, T. L.: MEaSUREs Greenland Surface Melt Daily 25km EASE-Grid 2.0, Version 1. Boulder, Colorado USA. NASA National Snow and Ice Data Center Distributed Active Archive Center. doi:10.5067/MEASURES/CRYOSPHERE/nsidc-0533.001. Accessed 1 September 2017, 2014.

Myers, P.G., Donnelly, C., and Ribergaard, M.H.: Structure and variability of the west Greenland Current in summer
470   derived from 6 repeat standard sections. Prog. Ocean., 80, 93-112, doi:10.1016/j.pocean.2008.12.003, 2009.

Noël, B., Fettweis, X., van de Berg, W.J., van den Broeke, M.R., and Erpicum, M.: Sensitivity of Greenland Ice Sheet surface mass balance to perturbations in sea surface temperature and sea ice cover: a study with the regional climate model MAR. Cryosphere, 8, 1871-1883, doi:10.5194/tc-8-1871, 2014.

475   Noël, B., van de Berg, W.J., van Wessem, J.M., van Mejgaard, E., van As, D., Lenaerts, J.T.M., Lhermitte, S., Munneke, P.K., Smeets, C.J.P., van Ulft, L.H., van de Wal, R.S.W., and van den Broeke, M.R.: Modelling the climate and surface mass balance of the polar ice sheets using RACMO2 – Part 1: Greenland (1958 – 2016). Cryosphere, 12, 811-831, doi:10.5194/tc-12-811, 2018.

Ohmura, A., and Reeh, N.: New precipitation and accumulation maps for Greenland. J. Glaciol., 37, 140-148, 1991.

Oltmanns, M., Straneo, F., and Tedesco, M.: Increased Greenland melt triggered by large-scale, year-round

480   precipitation events. Cryosphere Discuss., 1-18, doi:10.5194/tc-2018-243, 2018.

Onarheim, I.H., Eldevik, T., Smedsrud, L.H., and Stroeve, J.C.: Seasonal and regional manifestation of Arctic sea ice loss. J. Clim., 31, 4917-4932, doi:10.1175/JCLI-D-17-0427.1, 2018.

Overland, J.E., and Wang, M.: Recent extreme Arctic temperatures are due to a split polar vortex. J. Clim., 29, 5609-5616, 2016.

485   Peng, G., Meier, W.N., Scott, D.J., and Savoie, M.H: A long-term and reproducible passive microwave sea ice concentration data record for climate studies and monitoring, Earth Syst. Sci. Data, 5, 311–318, doi:10.5194/essd-5-311-2013, 2013.

Peng, G., Steele, M. Bliss, A.C., Meier, W.N., and Dickinson, S.: Temporal Means and Variability of Arctic Sea Ice Melt and Freeze Season Climate Indicators Using a Satellite Climate Data Record. Remote Sens., 10,

490   doi:10.3390/rs10091328, 2018.

Rennermalm, A.K., Smith, L.C., Stroeve, J.C., and Chu, V.W.: Does sea ice influence Greenland ice sheet surface-melt. Environ. Res. Lett., 4, 1-6, doi:107282/T36D5RDG, 2009.

Ribergaard, M.H.: Oceanographic investigations off west Greenland 2013. NAFO Scientific Council Documents, 14/001, 2014.

495   Serreze, M.C., and Stroeve, J.: Arctic sea ice trends, variability and implications for seasonal forecasting. Phil. Trans. R. Soc. A 373: 20140159, 2015.

van As, D., Fausto, R.S., and PROMICE Project Team: Programme for Monitoring of the Greenland Ice Sheet (PROMICE): first temperature and ablation records. Geol. Surv. Denmark Greenland Bull., 23, 73-76, 2011.

van As, D., Fausto, R.S., Steffen, K., and PROMICE project team: Katabatic winds and piteraq storms: observations

500   from the Greenland ice sheet. Geol. Surv. Denmark Greenland Bull., 31, 83-86, 2014.

van As, D., Hasholt, B., Ahlstrøm, A.P., Box, J.E., Cappelen, J., Colgan, W., Fausto, R.S., Mernild, S.H., Mikkelsen, A.B., Noël, B.P.Y., Petersen, D., and van den Broeke, M.R., 2018: Reconstructing Greenland Ice Sheet meltwater discharge through the Watson River (1949-2017). Arc., Antarc., and Alp. Res., 50, S100010, doi:10.1080/15230430.2018.1433799, 2018.

505   van de Wal, R.S.W., Smeets, C.J.P.P., Boot, W., Stoffelen, M., van Kampen, R., Doyle, S.H., Wilhelms, F., van den Broeke, M.R., Reijmer, C.H., Oerlemans, J., and Hubbard, A.: Self-regulation of ice flow varies across the ablation area in south-west Greenland, Cryosphere, 9, 603-611, doi:10.5194/tc-9-603, 2015.

van den Broeke, M.R., and Gallée, H.: Observation and simulation of barrier winds at the western margin of the Greenland ice sheet. Q.J.R. Meteorol. Soc., 122, 1365-1383, 1996.

510   van den Broeke, M., Smeets, P., Ettema, J.: Surface layer climate and turbulent exchange in the ablation zone of the west Greenland ice sheet. Int. J. Climatol., 29, 2309-2323, doi:10.1002/joc.1815., 2009.

van den Broeke, M.R., Enderlin, E.M., Howat, I.M., Kuipers Munneke, P., Noël, B.P.Y., van de Berg, W.J., van Meijgaard, E., and Wouters, B.: On the recent contribution of the Greenland ice sheet to sea level change. Cryosphere, 10, 1933-1946, doi:10.5194/tc-10-1933, 2016.

515   van den Broeke, M., Box, J., Fettweis, X., Hanna, E., Noël, B., Tedesco, M., van As, D., van de Berg, W.J., van Kampenhout, L.: Greenland ice sheet surface mass loss: Recent developments in observation and modeling. Curr. Clim. Change Rep., 3, 345-356, doi:10.1007/s40641-017-0084-8, 2017.

Smeets, P.C.J.P., Kuipers Munneke, P., van As, D., van den Broeke, M.R., Boot, W., Oerlemans, H., Snellen, H., Reijmer, C.H., and van de Wal, R.S.W: The K-transect in west Greenland: Automatic weather station data (1993-

520   2016). Arc., Antarc., and Alp. Res., 50, S100002, doi:10.1080/15230430.2017.1420954, 2018.

Straneo, F., and Heimbach, P.: North Atlantic warming and the retreat of Greenland's outlet glaciers. Nature, 504, 36-43, doi:10.1038/nature12854, 2013.

Stroeve, J.C., Mioduszewski, J.R., Rennermalm, A, Boisvert, L.N., Tedesco, M., and Robinson, D.: Investigating the local-scale influence of sea ice Greenland surface melt. Cryosphere, 11, 2363-2381, doi:10.5194/tc-11-2363,

525   2017.

Stroeve, J.C., Schroder, D., Tsamados, M., and Feltham, D.: Warm winter, thin ice? Cryosphere, 12, 1791-1809, doi:10.5194/tc-12-1791, 2018.

The Cryosphere
Discussions
Open Access

Tables

AWS Station	Network	Latitude (°N)	Longitude (°W)	Elevation (m asl)	Distance to/from terminus (km)
KAN_B	PROMICE	67.13	50.18	350	1
S5	IMAU	67.08	50.10	500	6
KAN_L	PROMICE	67.10	49.95	670	12
S6	IMAU	67.07	49.38	1000	37
KAN_M	PROMICE	67.07	48.84	1270	61
S9	IMAU	67.05	48.22	1500	88
KAN_U	PROMICE	67.00	47.03	1840	142

530

Table 1. Summary details of the PROMICE and IMAU AWS stations utilized in this study, including their approximate geographic position (in decimal degrees), elevation, and distance from the ice sheet terminus moving west to east. KAN_B is located on the tundra, roughly 1 km east of the terminus. Distances are rounded to the nearest km as AWS sites are known to move ~50-150 m year^{-1} (van de Wal et al., 2015).

535

AWS T Compare	T+ n[-60,-31]	T+ %[-60,-31]	T+ n[-30,-1]	T+ %[-30,-1]	T+ %[-60,-1]
S5 vs KAN_B	53	77	9	69	76
KAN_L vs KAN_B	32	46	8	62	49
S6 vs KAN_B	10	14	3	23	16
KAN_M vs KAN_B	2	3	1	8	4
S9 vs KAN_B	1	1	0	-	1
KAN_U vs KAN_B	0	-	0	-	-
∑ KAN_B T+ events	69	-	13	-	-

Table 2. Number of events (n), 2011-2015, and percent overlap (%) when KAN_B and S5, KAN_L, S6, KAN_M, S9, or KAN_U measured T≥0°C (i.e. T+). For example, 77% of the time in the 30 to 60-day window preceding ice cover the T≥0°C air temperature threshold at KAN_B is also observed at S5. The [-60,-31] and [-30,-1] periods reference time windows before respective annual dates of sea ice advance (DOA).

The Cryosphere
Discussions

Open Access

EGU
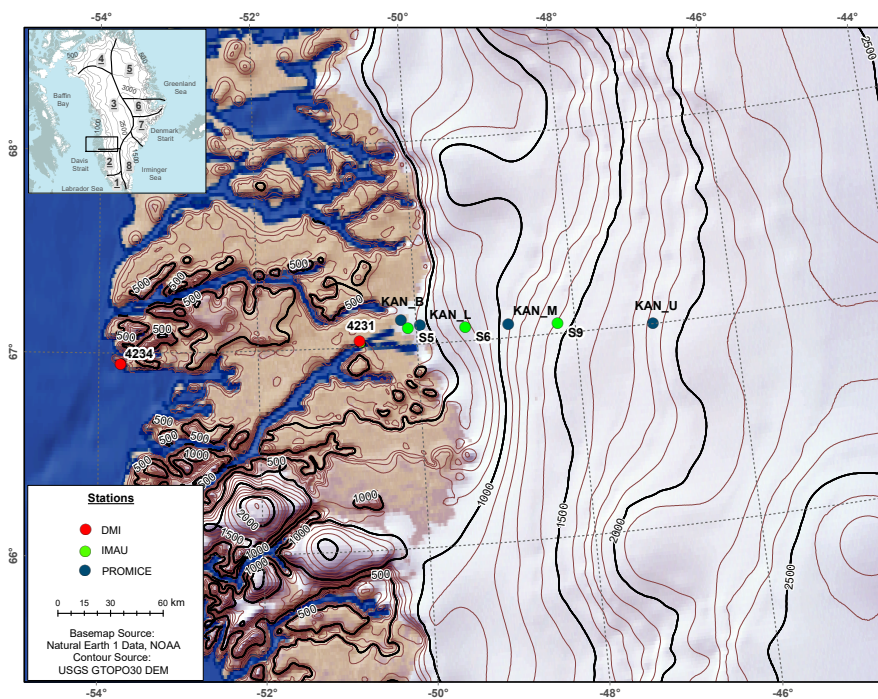
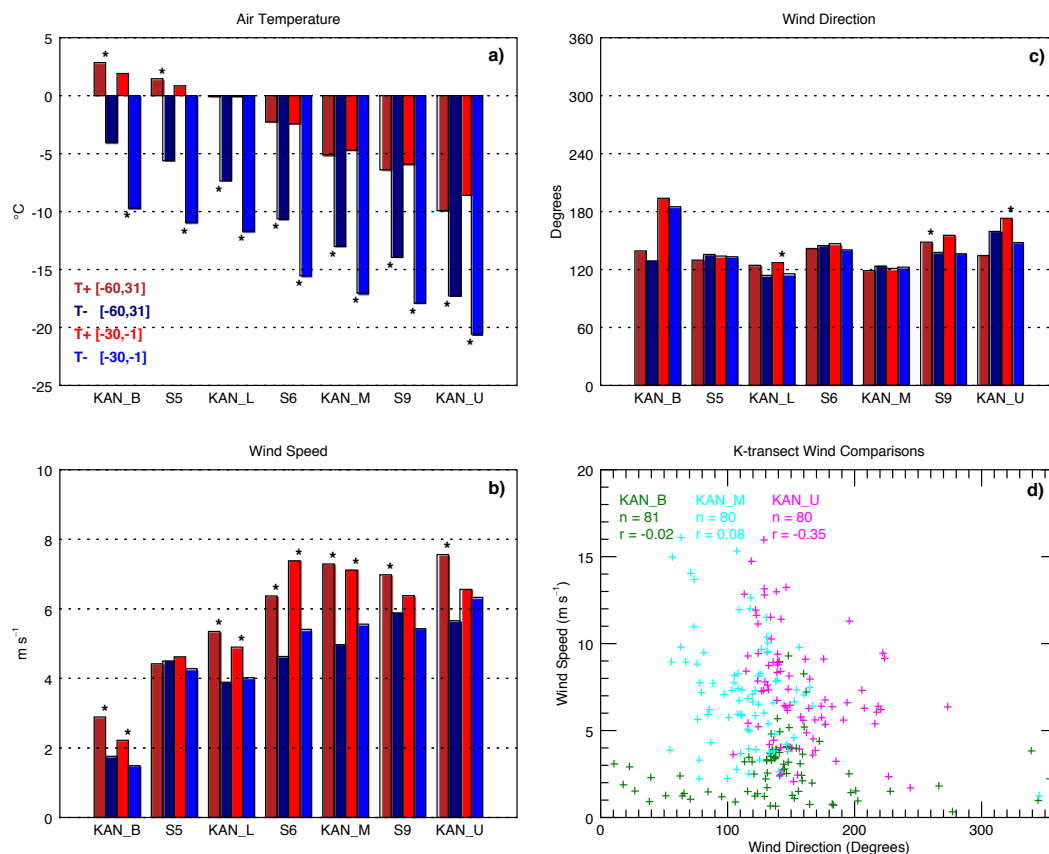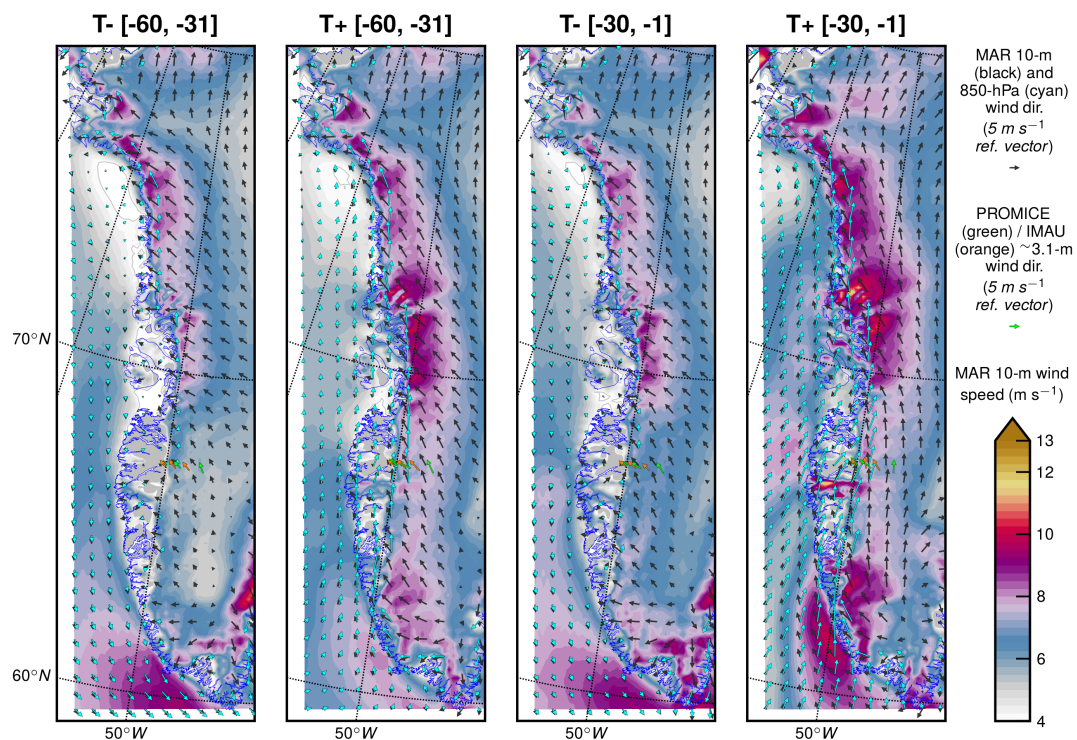**Figures**

Figure 1. Study area map with PROMICE and IMAU K-transect sites and adjacent terrestrial DMI stations (Kangerlussuaq (WMO code 4231) and Sisimiut (WMO code 4234)). The inset displays the northwest Atlantic Arctic region with superimposed GrIS topographically-defined boundaries, adopted from Ohmura and Reeh (1991).

545

The Cryosphere
Discussions

550

Figure 2. Composites of a) near-surface air temperature, b) wind speed, and c) wind direction for the T+ and T- events at KAN_B preceding Baffin DOA, 2011-2015. Significant differences ($p \leq 0.05$) between T+ and T- composites by time bins are shown by asterisks (*) between the bars. Panel d) shows wind speed as a function of direction for select, roughly equidistant K-transect PROMICE stations.

555

Figure 3. Composites of MAR 10-m (black arrows) and 850 hPa (cyan arrows) vector winds for the T+ and T- events
at KAN_B preceding Baffin DOA, 2011-2015. Wind observations from PROMICE (green arrows) and IMAU
(orange arrows) are overlaid for reference.
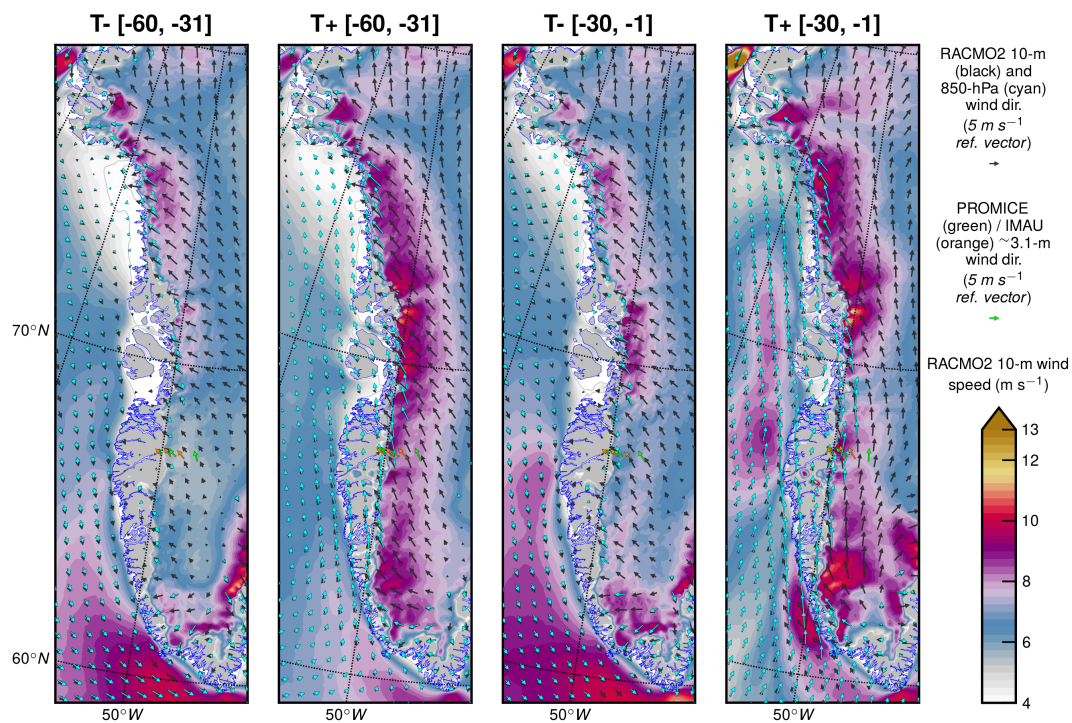
Figure 4. Composites of RACMO2 10-m (black arrows) and 850 hPa (cyan arrows) vector winds for the T+ and T-
565   events at KAN_B preceding Baffin DOA, 2011-2015 (refer to methods for details). Wind observations from
PROMICE (green arrows) and IMAU (orange arrows) are overlaid for reference.
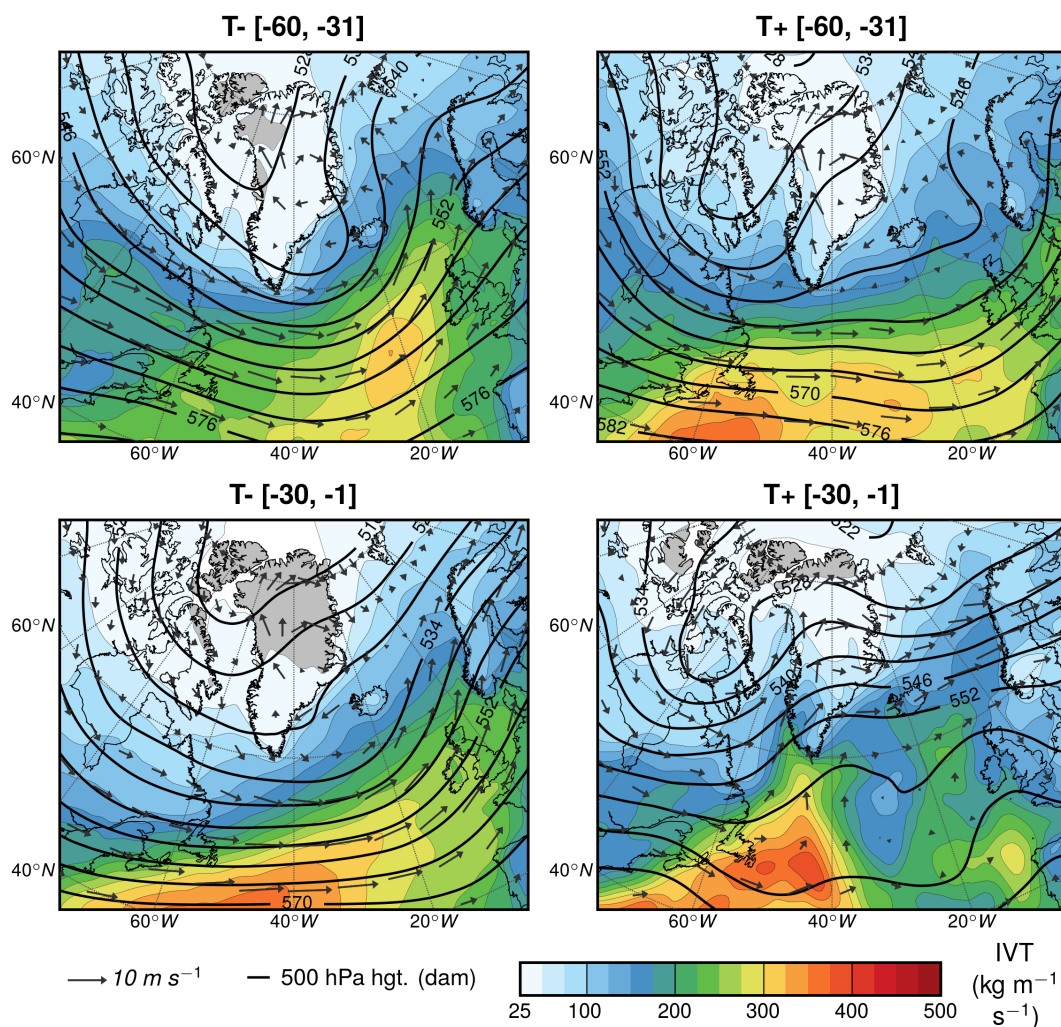
Figure 5. Composite plots of IVT, 1000-700 hPa winds, and 500 hPa GPH for T+ and T- events at KAN_B for the
two periods preceding DOA.
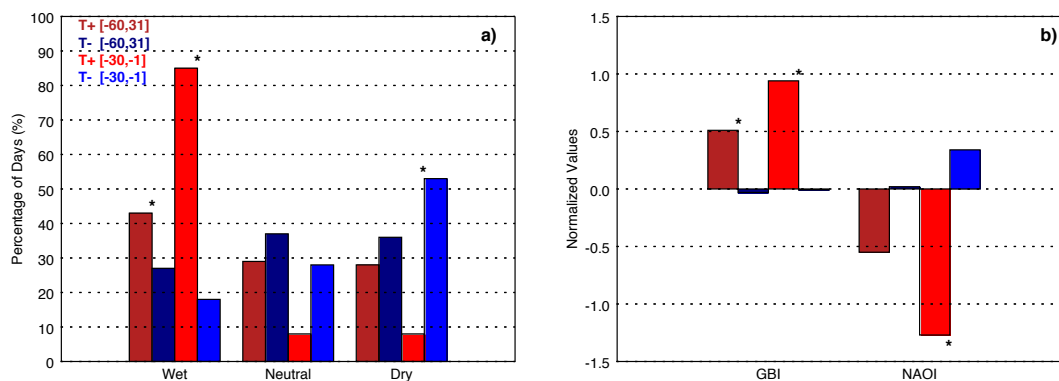
Figure 6. Composites of a) self-organizing map (SOM) nodes by wet, neutral and dry types (%) and b) normalized
GBI and NAO values (unitless) for T+ and T- events at KAN_B for the two periods preceding DOA. SOM aggregates
represent the ratio of each pattern's occurrence to the sum of all patterns for each time period and similarly colored
bars sum to 100%. Significant differences (p≤0.05) between T+ and T- composites by time bins are shown by asterisks
(*) between the bars.